

# **Supplementary data for “Injectable polypeptide hydrogel-based co-delivery of vaccine and immune checkpoint inhibitors improves tumor immunotherapy”**

Huijuan Song<sup>1</sup>, Pengxiang Yang<sup>1</sup>, Pingsheng Huang<sup>1\*</sup>, Chuangnian Zhang<sup>1</sup>, Deling Kong<sup>\*1, 2, 3</sup>,  
Weiwei Wang<sup>\*1, 4</sup>

<sup>1</sup> Tianjin Key Laboratory of Biomaterial Research, Institute of Biomedical Engineering, Chinese Academy of Medical Sciences and Peking Union Medical College, Tianjin 300192, China

<sup>2</sup> State Key Laboratory of Medicinal Chemical Biology, the Key Laboratory of Bioactive Materials, Ministry of education, College of Life Sciences, Nankai University, Tianjin 300071, China

<sup>3</sup> Jiangsu Center for the Collaboration and Innovation of Cancer Biotherapy, Cancer Institute, Xuzhou Medical University, Xuzhou 221004, Jiangsu, China

<sup>4</sup> State Key Laboratory of Molecular Engineering of Polymers (Fudan University), Shanghai 200433, China

## **Experiments and Methods**

### **In vivo biodistribution and clearance of anti-mouse PD-1 antibody**

To investigate the biodistribution and clearance of inhibitor antibody, APC/Fire<sup>TM</sup> 750-conjugated PD-1 antibody (Clone: 29F.1A12) with a maximum excitation at 650 nm and emission at 787 nm was used. Balb/c mice were received subcutaneous administration of 100 µg antibody loaded in (50 µL) or solubilized in PBS at the left flank. Three mice were used in each group. Antibody persistence at the injection site and drainage to lymph nodes were observed at several time points

post administration by an *in vivo* CRI Maestro imaging system (CRI Corporation, Woburn, MA, USA). Antibody decay kinetics was determined by quantifying the fluorescence intensity in pre-set regions of interest (ROI). The fluorescence signal was expressed as the percentage of the maximum recorded value, to show the percent decrease as a function of time. The distribution of antibody in major organs such as liver, spleen, lung and kidney was also examined by fluorescence imaging at pre-determined time points.

### **In vivo safety and toxicological profile**

To examine the *in vivo* safety of checkpoint inhibitors through systemic administration or local delivery by hydrogel, C57/BL6 mice were received intraperitoneal administration of anti-PD-1 (300  $\mu\text{g}$ ), and anti-CTLA-4 (300  $\mu\text{g}$ ) antibodies or subcutaneous injection of hydrogels loaded with the same amount of antibodies. Five mice were included in each group and untreated mice were used as controls. Acute toxicity was measured seven days later. Hepatotoxicity was measured by examining the serum level of alanine aminotransferase. Renal toxicity was checked by determining the blood urea nitrogen level. A complete blood count was also performed to identify any hematological toxicity by a blood cell analyzer. The number of leukocyte and platelet was counted, and the content of haemoglobin was tested.

## **Results**

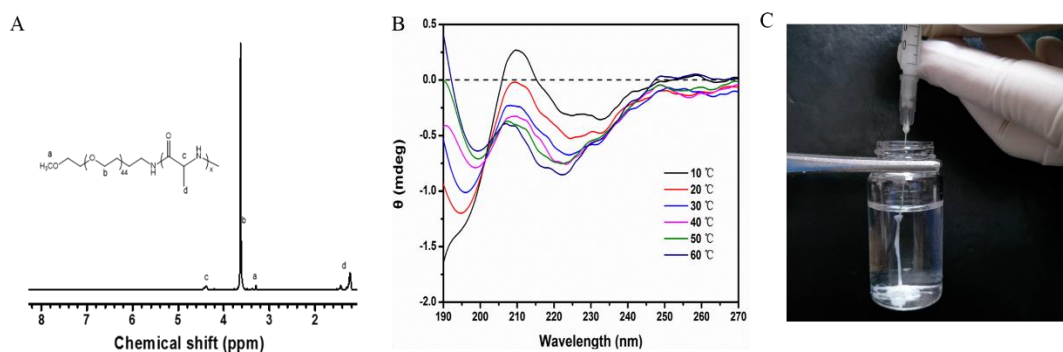


**Fig. S1 Characterization of PEG-*b*-poly(L-alanine) copolymer.** (A) The <sup>1</sup>H NMR spectrum (solvent, CF<sub>3</sub>COOD) of copolymer and (B) the CD curves of copolymer dissolved in water at a concentration of 0.1 mg/mL. The secondary structure was recorded in the temperature range of 10-60 °C. (C) The injectability of PEA hydrogel through a syringe.

Table S1 The physicochemical characters of PEA copolymer

Polymer	PEG <sup>a</sup>	p(L-alanine) <sup>a</sup>	<i>M<sub>n</sub></i> <sup>a</sup>	PDI <sup>b</sup>	CAC (mg/mL) <sup>c</sup>
PEA	44	10	2710	1.12	2.27×10 <sup>-4</sup>

<sup>a</sup> The polymerization degree calculated by <sup>1</sup>H NMR. <sup>b</sup> Determined by GPC. <sup>c</sup> Critical aggregation concentration (CAC), measured by pyrene-based fluorescence spectrometry.

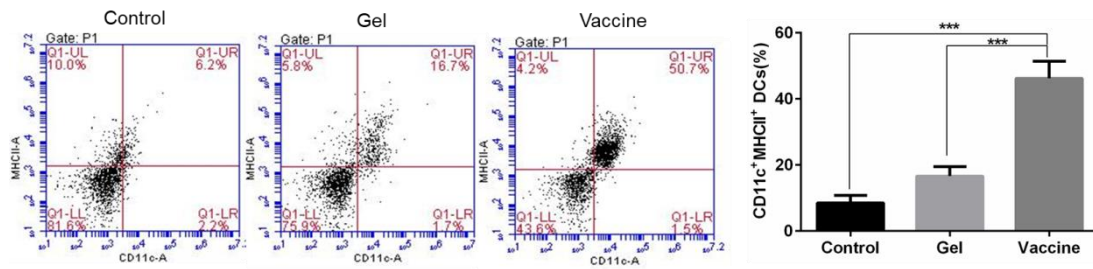


**Fig. S2 In vitro DC maturation induced by the polypeptide hydrogel-based vaccine.** BMDCs were treated by blank hydrogels (Gel) or hydrogels containing TCL and GM-CSF (Gel+TCL+GM-CSF), stained by CD11c and MHCII antibodies and analyzed by flow cytometry. The statistical significance was analyzed by one-way ANOVA. \*\*\**p*<0.001, between indicated groups.

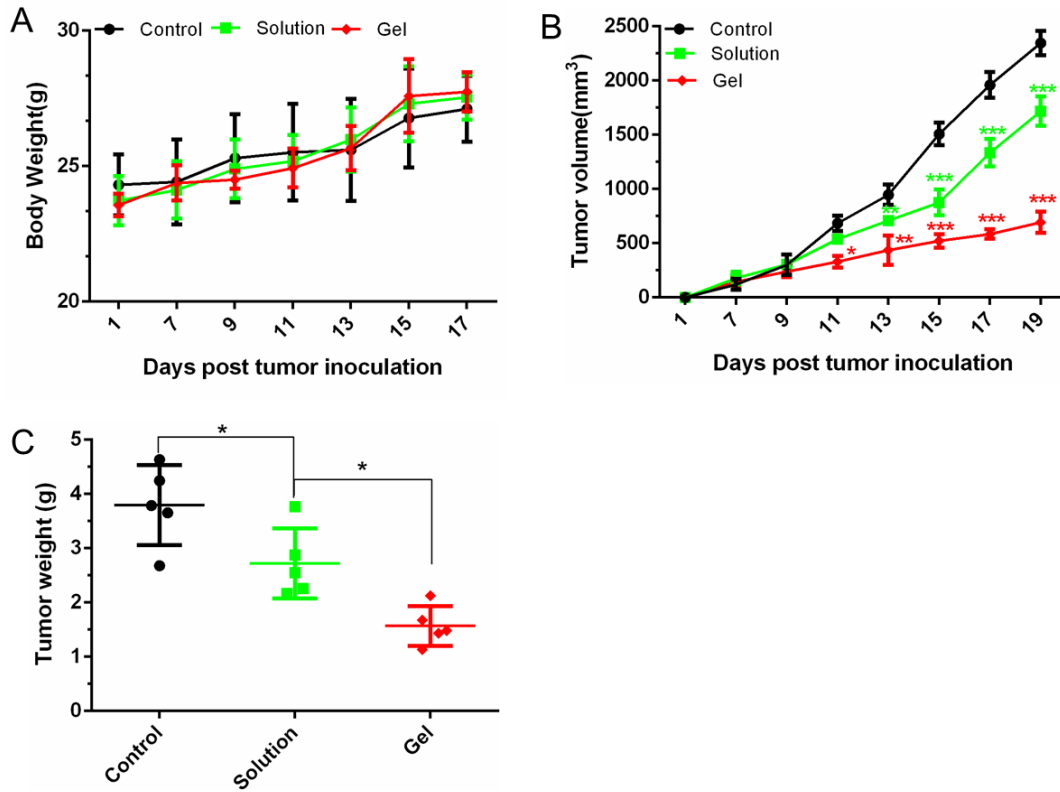


**Fig. S3 Antitumor efficiency of the combination of vaccine and checkpoint inhibitors formulated in solution or hydrogel.** (A) The profile of animal body weight post-tumor inoculation. (B) The curve of tumor volumes. The statistical difference between Solution and Control, or Gel group was calculated by using two-way ANOVA method in GraphPad Prism software, which was labeled in green and red asterisk, respectively; \* $P < 0.05$ , \*\* $P < 0.01$  and \*\*\* $P < 0.001$ . (C) Mass weight of tumors excised at day 17. Data are shown as mean  $\pm$  SDs ( $n = 6$ ). \* $P < 0.05$ , between indicated groups.

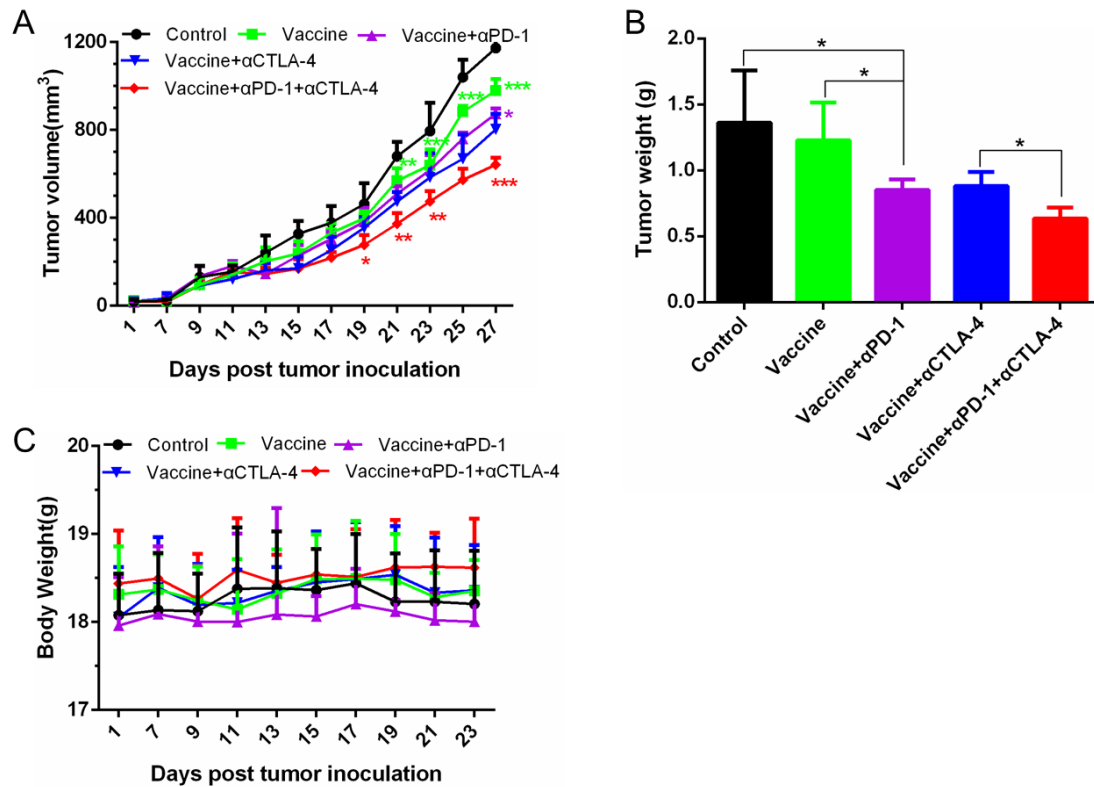


**Fig. S4 Hydrogel-based co-delivery of vaccine and dual checkpoint inhibitors induced potent therapeutic efficiency against 4T1 tumor.** (A) The curve of tumor volumes. Data are shown as mean  $\pm$  SDs (n=6). The statistical difference between Vaccine and Control, Vaccine+ $\alpha$ PD-1 and Vaccine, or Vaccine+ $\alpha$ PD-1+ $\alpha$ CTLA-4 and Vaccine+ $\alpha$ CTLA-4 group was calculated by using two-way ANOVA in GraphPad Prism software, which was labeled in green, purple and red asterisk, respectively; \* $P$ <0.05, \*\* $P$ <0.01 and \*\*\* $P$ <0.001. (B) Mass weight of tumors excised at day 27. \* $P$ <0.05, student's  $t$ -test, between indicated groups. (C) The profile of animal body weight post-tumor inoculation.

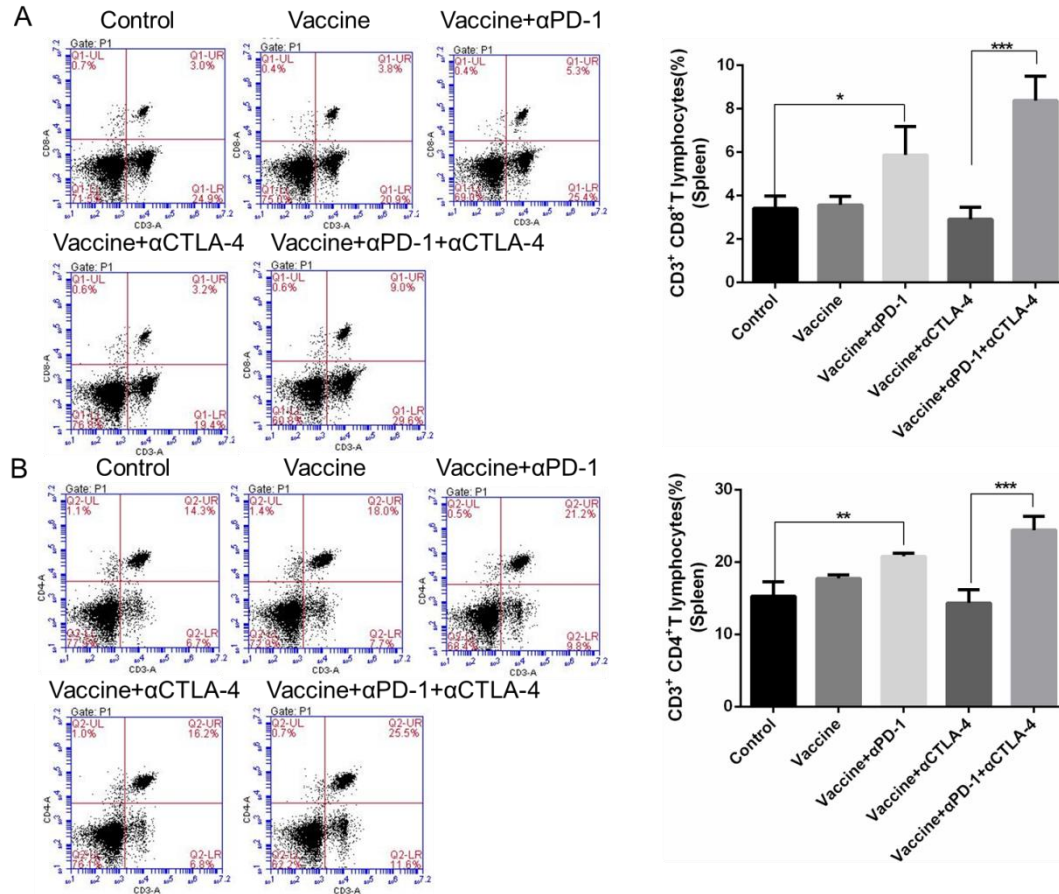


**Fig. S5 Hydrogel-based co-delivery of vaccine and checkpoint inhibitors enhanced the systemic T-cell response in 4T-1 tumor-bearing mice.** (A, C) Ratio of CD8<sup>+</sup> T (A) or CD4<sup>+</sup> T (C) cells isolated from the spleens of untreated tumor-bearing mice (control) and mice treated with blank hydrogels (gel) or hydrogel vaccines (vaccine) alone, or in combination with either anti-PD-1 (+αPD-1) or anti-CTLA-4 (+αCTLA-4) antibodies or with dual antibodies (+αPD-1+αCTLA-4). (B, D) The ratio of IFN-γ<sup>+</sup>CD8<sup>+</sup> T (B) or IFN-γ<sup>+</sup>CD4<sup>+</sup> T (D) cells to the total number of CD8<sup>+</sup> T or CD4<sup>+</sup> T cells in the spleens as determined by flow cytometry. Data are shown as mean ± SDs (n=4). \**P*<0.05, \*\**P*<0.01 and \*\*\**P*<0.001, between indicated groups.

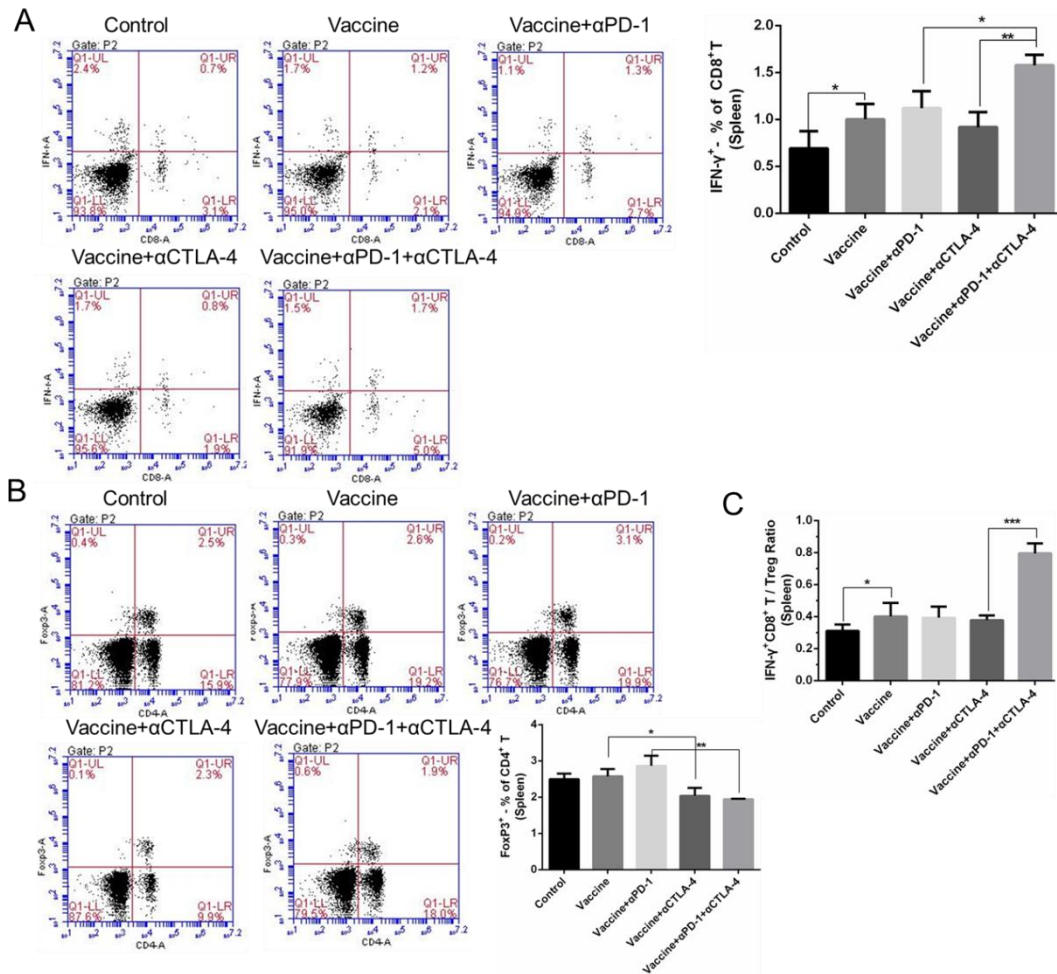


**Fig. S6 Hydrogel-based co-delivery of vaccine and checkpoint inhibitors enhanced the activation of systemic CD8<sup>+</sup> T-cells and increased the ratio of IFN- $\gamma$ <sup>+</sup> CD8<sup>+</sup> T cells/Tregs in 4T1 tumor-bearing mice.** (A) Representative flow cytometry profiles of IFN- $\gamma$  and CD8 staining and quantification analysis of IFN- $\gamma$ <sup>+</sup> CD8<sup>+</sup> T cells in the spleens. (B) Representative flow cytometry profiles of FoxP3 and CD4 staining and quantification analysis of FoxP3<sup>+</sup>CD4<sup>+</sup> T cells in the spleens. (C) Ratios of IFN- $\gamma$ <sup>+</sup>CD8<sup>+</sup> T cells to Tregs. Data are shown as mean  $\pm$  SDs (n=4).

\* $P < 0.05$ , \*\* $P < 0.01$  and \*\*\* $P < 0.001$ , between indicated groups.

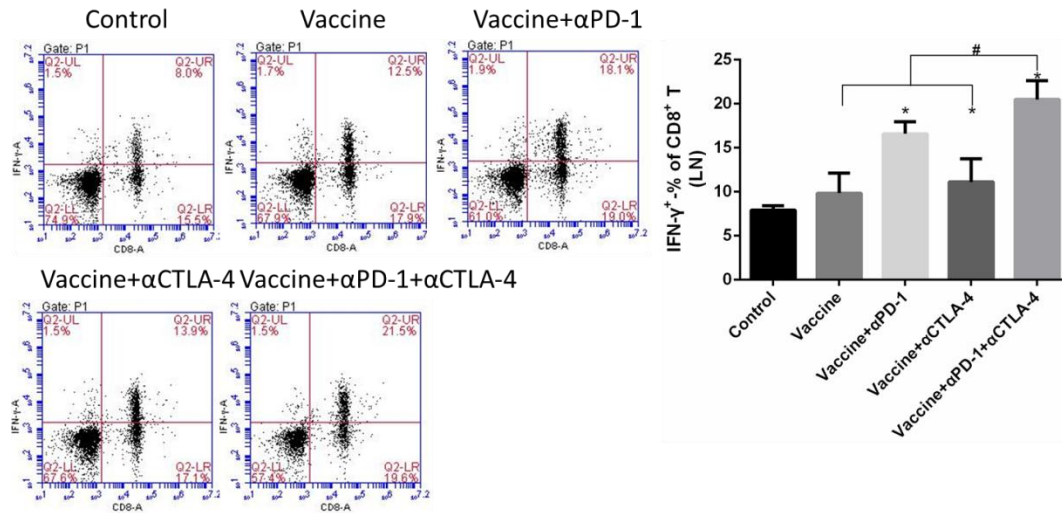


**Fig. S7 Hydrogel-based combination therapy activated CD8<sup>+</sup> T cells in the local lymph node (LN).** (Left) Representative flow cytometry profiles of IFN- $\gamma$  and CD8 staining and (right) quantification analysis of IFN- $\gamma$ <sup>+</sup> CD8<sup>+</sup> T cells within the LN. Data are shown as mean  $\pm$  SDs (n=3). \**P*<0.05, versus the control; #*P*<0.01, between indicated groups.

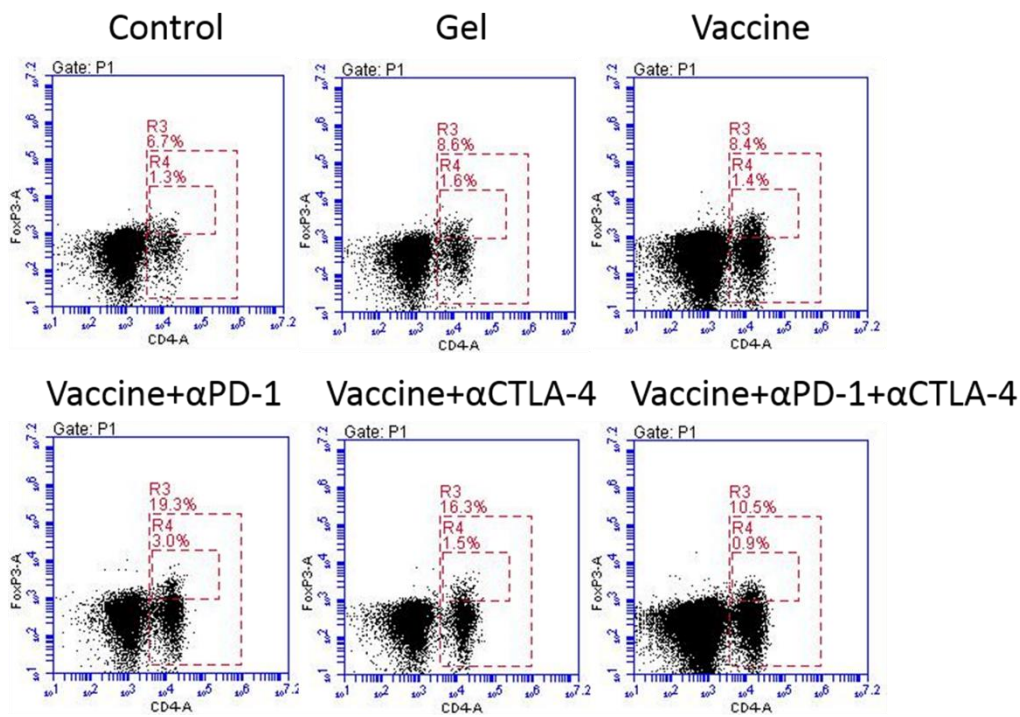


**Fig. S8 Representative flow cytometry profiles of FoxP3 and CD4 staining shown in dot plots.**

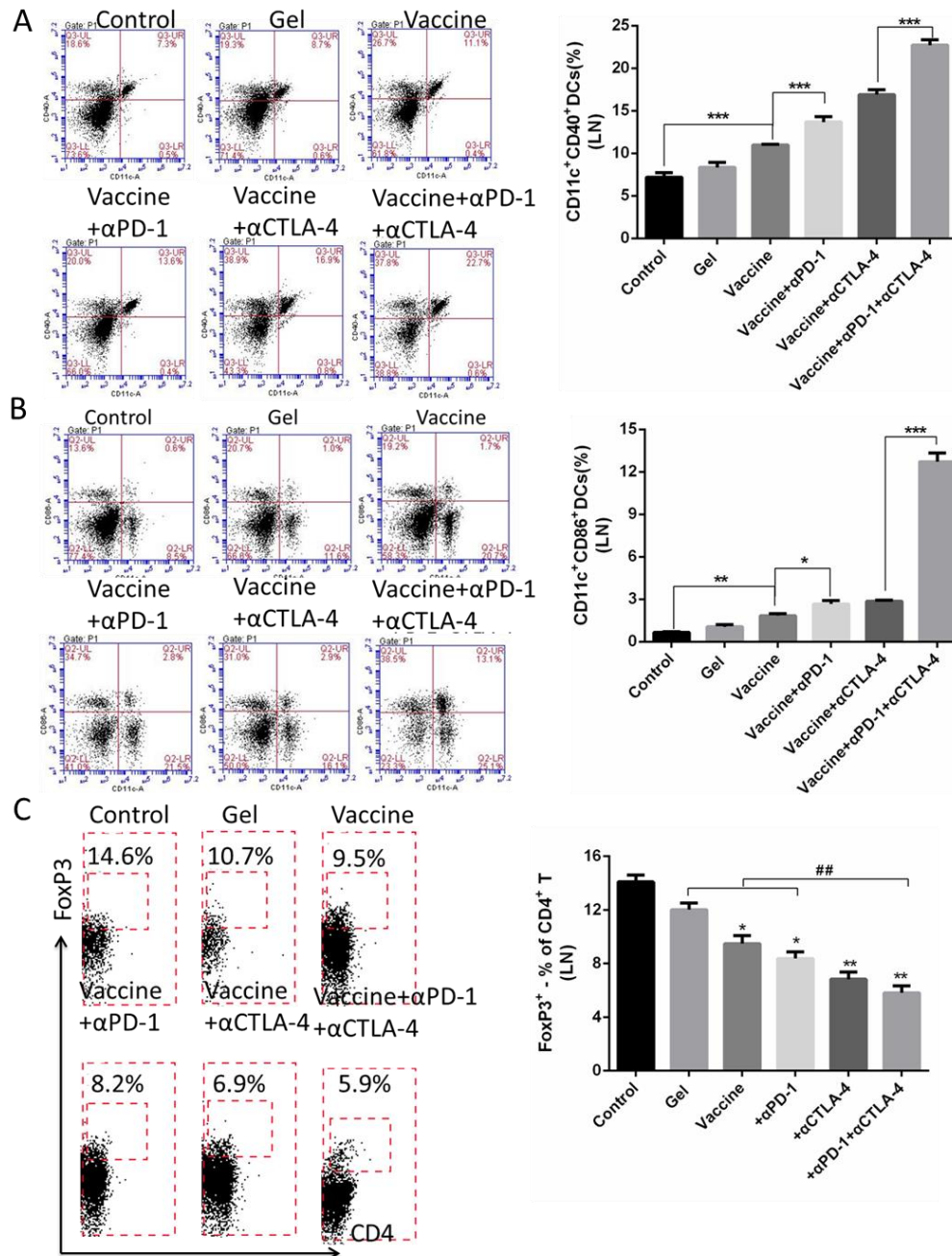


**Fig. S9** Combination therapy activated DCs and decreased the ratio of Tregs in the draining lymph nodes (dLNs) of melanoma-inoculated mice. (A, B) Representative flow cytometry profiles of CD40 (A) and CD86 (B) staining and the quantification analysis of CD40<sup>+</sup>CD11c<sup>+</sup> or CD86<sup>+</sup>CD11c<sup>+</sup> DCs within dLNs. Data are shown as mean  $\pm$  SDs (n=3). \* $P$ <0.05, \*\* $P$ <0.01 and \*\*\* $P$ <0.001, between indicated groups. (C) Analysis of Tregs in the dLNs by FoxP3 and CD4 staining. Data are shown as mean  $\pm$  SDs (n=3). \* $P$ <0.05, and \*\* $P$ <0.01, versus the control; ## $P$ <0.01, between indicated groups.

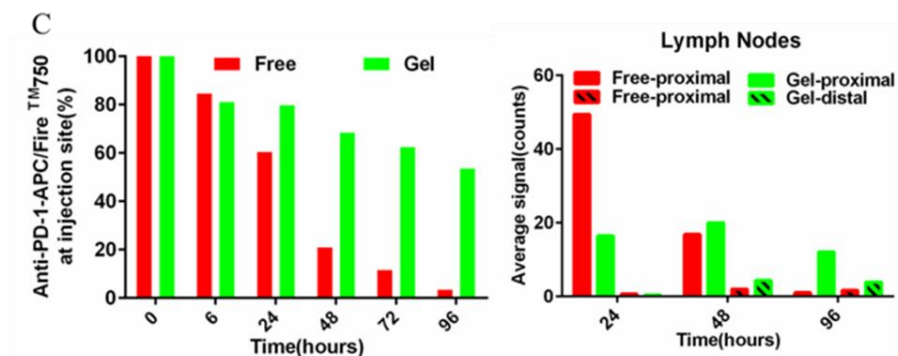
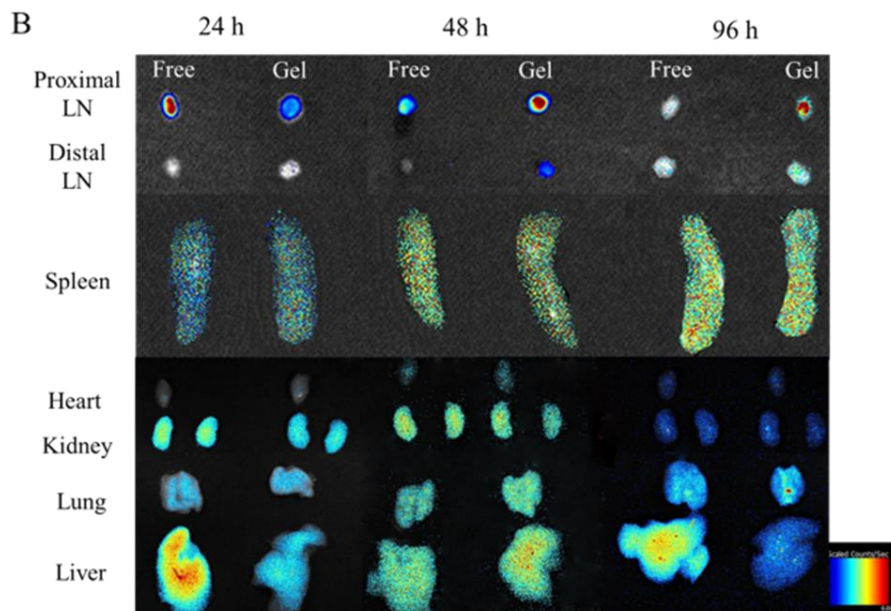
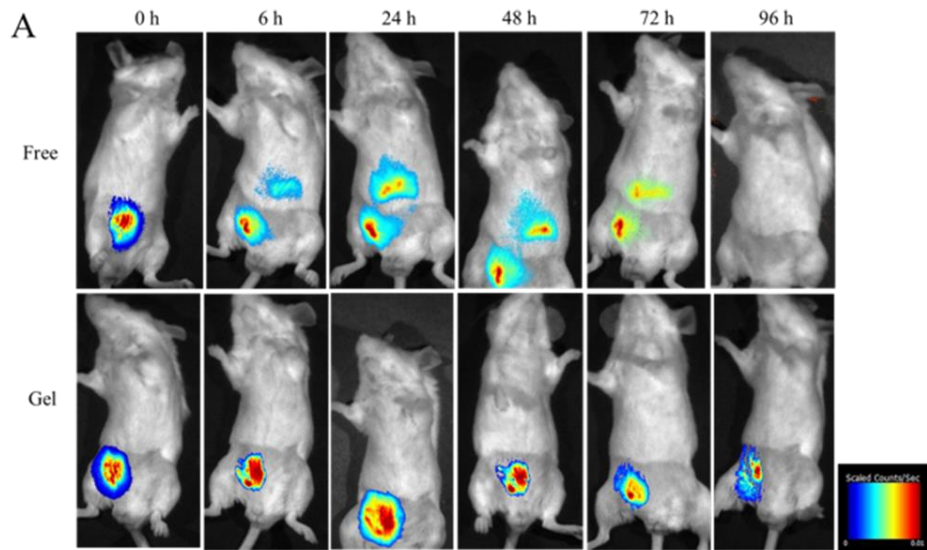


**Fig. S10** In vivo distribution and clearance of anti-PD-1 antibody delivered by polypeptide hydrogel (Gel group) or injected in solution (Free group). (A) Representative images of antibody duration in the injection site and (B) antibody distribution in major organs including

lymph node (LN), spleen, liver, heart, lung and kidney. (C) The fluorescence intensity of antibody at the injection site (left, normalized to the fluorescence intensity captured just after injection) and at the lymph nodes (right, average signal counts were recorded.) Data are shown as mean values. APC/Fire<sup>TM</sup>750-conjugated PD-1 antibody was used.

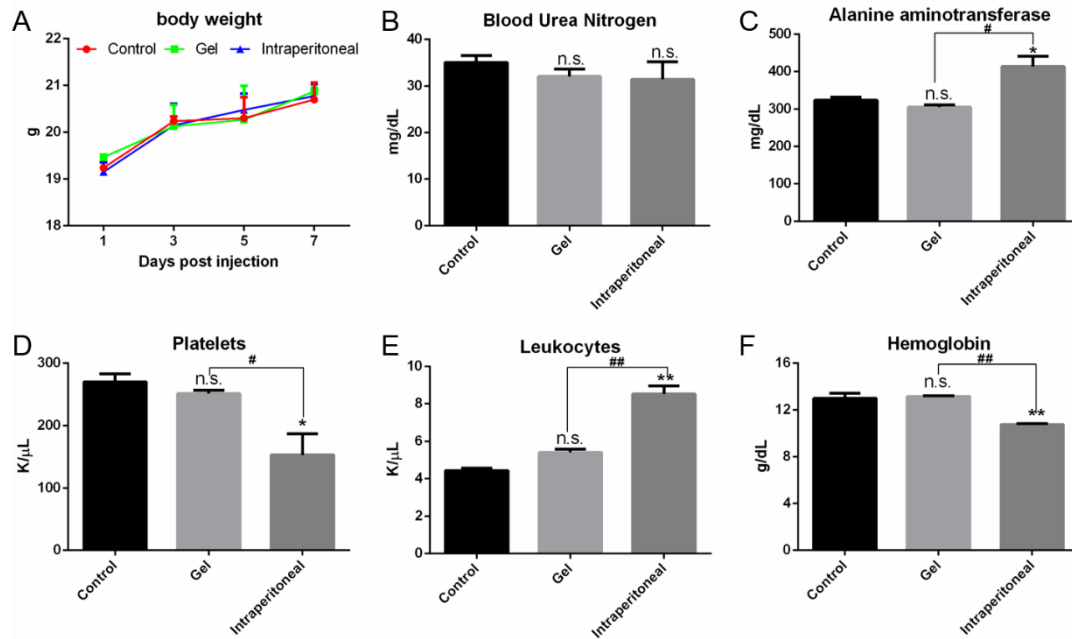


**Fig. S11 In vivo safety and toxicological analysis of anti-PD-1 antibody delivered by polypeptide hydrogel (Gel group) or injected intraperitoneally in solution (Intraperitoneal group).** (A) Mice body weight determined at day 1, 3, 5, and 7. (B, C) The level of blood urea nitrogen (B) and alanine aminotransferase (ALT, C) determined seven days after antibody administration. (D-F) Hematological toxicity indicated by the count of platelets (D) and leukocytes (E) and the content of hemoglobin (F). \* $P < 0.05$ , and \*\* $P < 0.01$ , versus the control; # $P < 0.05$ , and ## $P < 0.01$ , between indicated groups; n.s. = not significant.